FEM Analysis of RF Breast Ablation: Multiprobe *versus* Cool-tip Electrode

V. QUARANTA[1], G. MANENTI[2], F. BOLACCHI[2], E. COSSU[2], C.A. PISTOLESE[2], O.C. BUONOMO[2], L. CAROTENUTO[1], C. PICONI[1] and G. SIMONETTI[2]

[1]*Tecnobiomedica S.p.A. Via Vaccareccia 41, 00040 Pomezia, Rome;*
[2]*Department of Diagnostic and Molecular Imaging, Radiation Therapy and Interventional Radiology, University Hospital Policlinico Tor Vergata (PTV), Rome, Italy*

Abstract. *Background: Radio-frequency ablation (RFA) has recently received much attention as an effective minimally invasive strategy for the local treatment of tumors. The purpose of this study was to evaluate the efficacy of single-needle cool-tip RF breast ablation in terms of temperature distribution and duration of the procedure as compared to multiprobe RF breast ablation. Materials and Methods: Two different commercially available radiofrequency ablation needle electrodes were compared. Finite-element method (FEM) models were developed to simulate the thermoablation procedures. A series of ex vivo radiofrequency thermal lesions were induced to check the response of the FEM calculations. Results: Data obtained from FEM models and from ex vivo procedures showed that cool-tip RF breast ablation assures better performances than multiprobe RF breast ablation in terms of temperature distribution and duration of the procedure. Histopathological analysis of the cool-tip RF thermoablated specimens showed successful induction of coagulation necrosis in the thermoablated specimens. Conclusion: Data obtained from FEM models and from ex vivo procedures suggest that the proposed cool-tip RF breast ablation may kill more tumor cells in vivo with a single application than the multiprobe RF breast ablation.*

Surgical breast cancer treatment is effective, but is a highly invasive procedure. Because of the poor cosmetic result of such invasive therapy, treatments that would preserve the greatest amount of normal tissue have great appeal especially for the treatment of early diagnosed cancers (small tumors). Thus, the demand for novel minimally invasive techniques for the treatment of breast cancer has grown during recent years. Radio-frequency (RF) ablation has recently received much attention as an effective minimally invasive strategy for the local treatment of solid malignancies (1, 2). Although other methods of thermal ablation such as laser, microwave and High Focused Ultrasound (HIFU) are being performed, RF is currently receiving the greatest attention in the light of several factors: its general availability, the recent technical advances facilitating its use and the active marketing on the part of manufacturers.

To accomplish RF tumor ablation, an "RFA probe" (usually 14 to 21 gauge needle-like electrodes) is placed directly into the target tissue with the use of ultrasound (US) imaging guidance (2, 3).

An RF generator produces an RF voltage between the active electrode and a reference electrode (usually a large conductive pad in contact with the patient's skin), thereby establishing lines of electric field within the patient's body between the two electrodes. At the low RF used for this procedure (460-550 kHz), the electric field pattern is governed essentially by electrostatic equations. Essentially, the electric field oscillates with the alternating RF current, which causes oscillatory movement of ions in the target tissue in proportion to the field intensity. The mechanism of tissue heating for RF ablation is frictional. Tissue heating occurs as a result of ionic agitation surrounding the electrode as the RF current oscillates while reaching its ground (reference electrode). It is the generation of tissue heating that induces cellular death *via* thermal coagulation necrosis. Therefore, the volume of RF heat ablation is governed by the temperature distribution within the tissue (3). Between 60˚C and 100˚C, near instantaneous induction of protein coagulation that irreversibly damages key cytosolic and

Correspondence to: (i) Dr. Eng. Vincenzo Quaranta, Tecnobiomedica S.p.A., Via Vaccareccia 41, I-00040 Pomezia, Rome, Italy. e-mail: v.quaranta@tecnobiomedica.it. (ii) Dr. G. Manenti, Department of Diagnostic and Molecular Imaging, Radiation Therapy and Interventional Radiology, University Hospital Policlinico Tor Vegata (PTV), Viale Oxford 81, 00133 Rome, Italy. e-mail: guggi@tiscali.it

Key Words: RFA, RF ablation, breast ablation, Finite-element method, FEM, cool-tip electrode, multi-probe.

Table I. *Thermoelectric properties of tissue.*

Tissue	Density (Kg/m^3)	Thermal capacity [J/(˚C Kg)]	Thermal conductivity [W/(m ˚C)]	Electrical conductivity (Siemens/ meter)	Permittivity
Liver	1060	3628	0.465	0.148	2957
Fat (Breast)	940	2600	0.2	0.025	35

mitochondrial enzymes and nucleic acid-histone complexes occurs (4, 5).

A key limitation so far for RF ablation has been creating adequate volumes of tissue destruction. Several methods have been investigated to increase lesion size.

Multiprobe monopolar RF needles with multiple thin, curved electrodes that extend from a central cannula have been successfully used for RF liver ablation (6) and are currently employed for RF breast ablation (7, 10). Also, bipolar RF ablation using two active needle electrodes has been suggested (11). Recently, monopolar single-needle cool-tip electrodes have been successfully used to induce a consistent necrosis volume in tumors other than breast tumors (12, 13).

The purpose of this study was to evaluate the efficacy of cool-tip electrode RF breast ablation in terms of temperature distribution and duration of the procedure as compared with conventional multiprobe RF breast ablation.

Materials and Methods

Finite-element method (FEM) models. Five FEM models have been developed: Model 1: breast tissue, multiprobe LN electrode, power-controlled mode; Model 2: liver tissue, multiprobe LN electrode, power-controlled mode; Model 3: breast tissue, Miras PTV cool-tip electrode, power-controlled mode; Model 4: breast tissue, multiprobe Miras LN electrode, temperature-controlled mode; and Model 5: breast tissue, cool-tip Miras PTV Electrode, temperature-controlled mode.

Solving method. FEM Models were implemented and developed using FEMLAB (Comsol, Burlington MA, USA) on a 3.0 GHz Intel Pentium IV, with 1 Gbyte RAM. The model consisted of 64 034 tetrahedral elements and 12 880 nodes nonuniform mesh; mesh size close to the probe was 0.2 mm and at the model boundaries was 5 mm. Convergence tests had been performed to ensure adequate spatial resolution. The time steps during the solving analysis of the FEM started at 0.05 sec and were subsequently automatically controlled by the solver software so that the maximum temperature change during each step was less than 3˚C.

Boundary conditions. In all models the boundary conditions were the same.

Table II. *Results from the experimental ex vivo tests.*

Test No.	Electrode	Tissue type	Power (W)	Time (sec)	Max T (˚C) External thermocouple (deployed - 3.0 cm)
1				237	94
2	LN		20	224	96
3		Swine		308	106
4		mammary		444	120
5	PTV		20	384	118
6				603	128
7		Bovine		1165	120
8	LN	liver	20	874	120
9				797	120
10				332	95
11	LN	Human	20	470	104
12		breast		354	92
13				626	113
14	PTV		20	707	119
15				778	128

i. Temperature boundary conditions: For the surface of the cylinder the temperature value was kept costant at 37˚C. Since the thermal mass of the probe was less than that of the saline, we assumed that heat conduction into the probe itself was minimal. Thus, for all other surfaces, the thermally insulating boundary condition $n\cdot(k\nabla T)=0$ was applied. Only the active surface of the cooled electrode was set to the cooling media temperature, T=5˚C.

ii. Electrical boundary conditions: For each of the outer surfaces of the model, an electrical boundary condition of V=0 was applied, to simulate the return ground electrode. A source potential (Vo) was applied to the conducting areas of the probe. The non-conducting portions were given an insulating boundary condition such that $n\cdot(\sigma\nabla V)=0$; where n is the unit vector normal to the surface, σ is the electrical conductivity and V is the voltage at the insulating surface.

Tissue properties. Tissue thermal and electrical properties used for the models have been previously described (14-22) and are reported in Table I. Breast tissue is a mixture of fat, glandular and connective tissues. Since fat has the lowest thermal conductivity of all, due to the low water content, the model was simplified considering all the breast tissue to be adipose tissue.

Model geometry. Three-Dimensional FEM Analyses. FEM models of Miras PTV (Single cooled needle) (Figure 1a), by University Hospital Policlinico Tor Vergata (PTV) (Rome, Italy) in collaboration with INVATEC Srl (Rocadelle, Brescia, Italy) and Miras LN (Multiprobe) (Figure 1b), by INVATEC Srl were developed. The active portion of each probe was embedded into a cylindrical region (height: 12.0 cm/diameter: 10.0 cm) that simulated tissue surrounding the probe. Due to the symmetry of the model, computing time was saved by modelling a quarter of the cylinder only. The axial-symmetric assumption required axial-symmetry of geometry, materials, loadings and boundaries, which also led to an axial-symmetric solution.

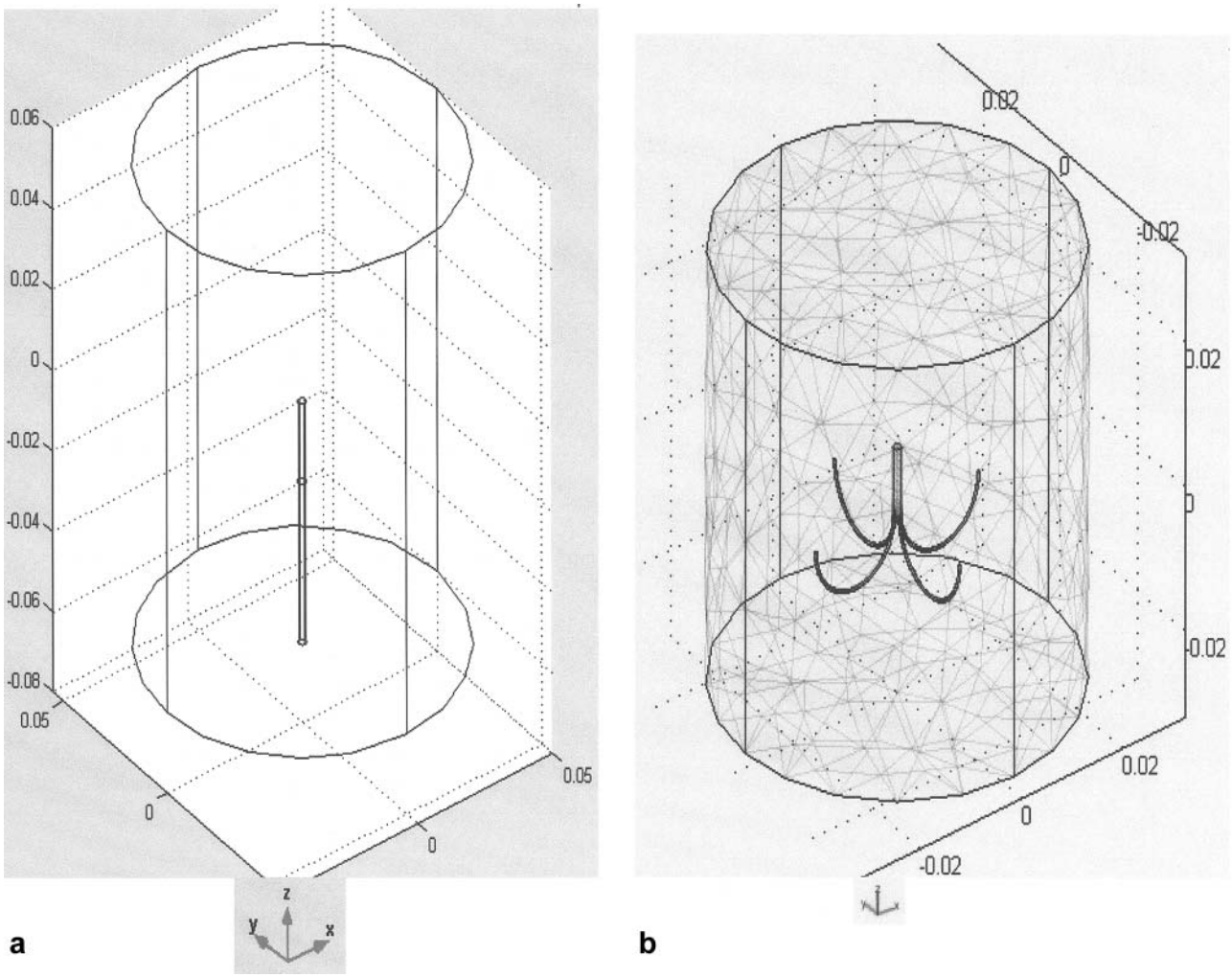

Figure 1. *FemLab FEM models: a) Miras PTV Cool-tip Electrode and b) Miras LN Multiprobe Electrode.*

The bioheat equation. The potential and temperature distributions in the tissues were monitored using the protocols reported in the literature. Briefly, it was assumed that the ablation probe dissipated the majority of its energy through electrical conduction. In this situation a quasi-static electrical conduction model was assumed, which allowed the use of Laplace's equation to solve the electric field (16). The expression for the electric potential (V) was solved quickly over the entire volume and the value was implemented into the source term of the heat conduction equation, the so-called bioheat equation (16-19). The energy generated by the metabolic processes was ignored, Q_m (W/m) and the blood perfusion contribution considered insignificant.

Energy delivery schemes. Three of the five simulations were performed with the power-controlled ablation mode. The erogation power was set to deliver an average energy of 30 W until a final tissue temperature of 100˚C (charring temperature) was reached. Two models simulated the temperature-controlled ablation mode. Power value was initially set at 30 W and adjusted to maintain a temperature of 90˚C for eight minutes. At the end of the soak time, power modulation was stopped and the last power value applied was maintained until a final temperature of 100˚C was reached. Temperature distributions were recorded during the procedure.

Ex vivo experiments. Tissue samples: three tissue types were tested (Figures 2 and 3). For each tissue type, six samples were obtained (10 cm long x 10 cm wide x 5 cm thick).

Tissues used were swine mammary tissue, from two adult non-nursing female pigs; bovine liver tissue, from a young calf's liver and human breast tissue from excised breast mastectomy specimens.

Radiofrequency system. A 460-kHz generator (Fogazzi, Concesio, Italy) capable of 100 W maximum output power at 200 Ω (Figure 4a) was used to perform the tests using two types of electrodes Miras PTV (monopolar cool-tip single needle) (Figure 4c) and Miras LN (monopolar multiprobe needle) (Figure 4d). The Miras LN is a multiprobe stainless steel electrode equipped with four active hooks (0.5 mm diameter). The Miras PTV is a monopolar 200 mm two

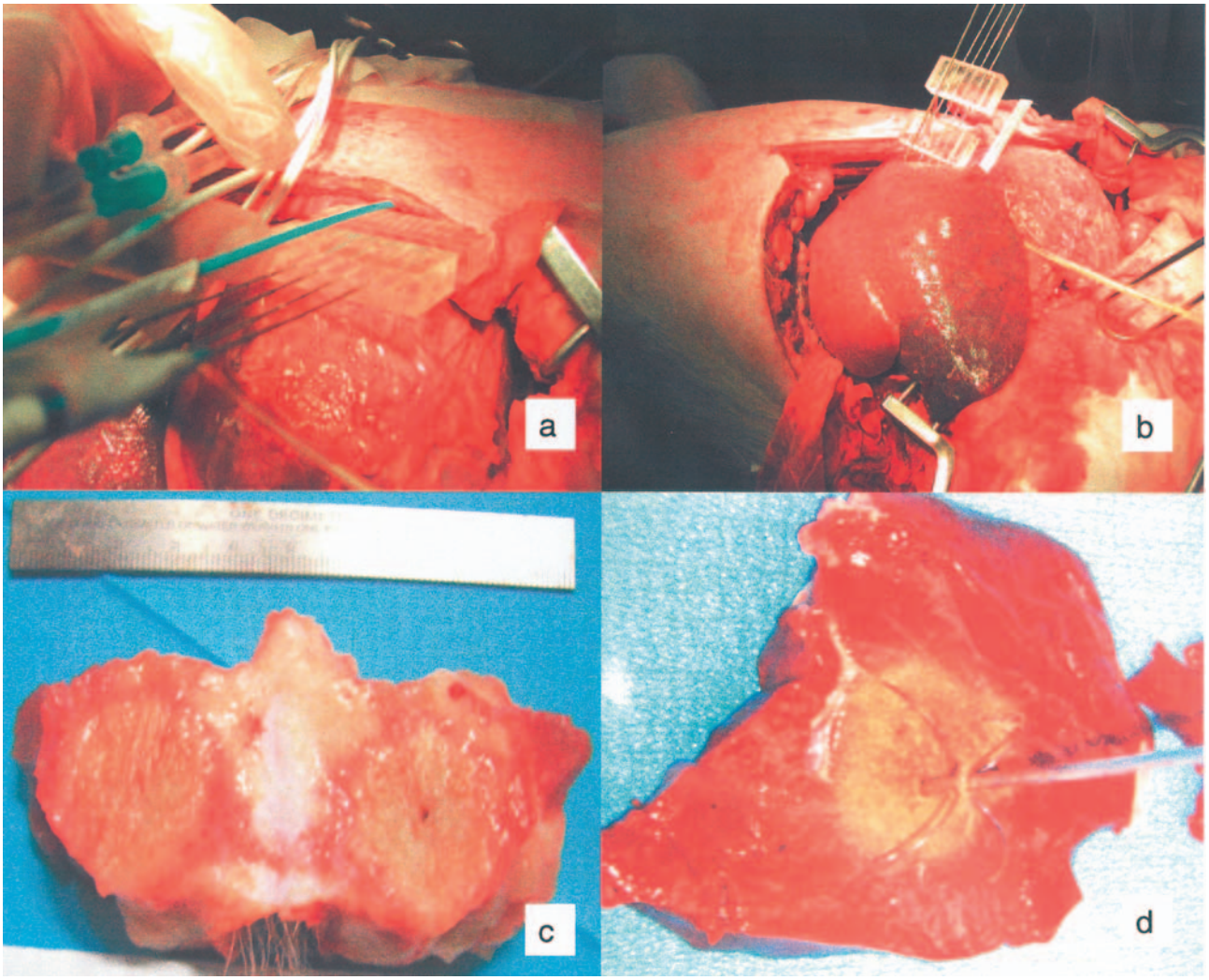

Figure 2. *a) Swine mammary sample during Miras PTV cool-tip RFA, b) calf liver sample during Miras LN multiprobe RFA, c) macroscopic appearance of an excised swine mammary specimen after RFA and d) macroscopic appearance of an excised calf liver specimen after RFA.*

lumens single electrode with active stainless steel tip exposure of 25 mm (Figure 4c). The two lumens were equipped with connectors for inflowing and outflowing of chilled saline solution, which permitted continuous internal cooling. A peristaltic pump (Fogazzi) cooled the electrode internally by delivering a chilled saline perfusion (Na-Cl 38% 2000 ml at 0˚C) through its cannula sheath, providing optimal cooling of the electrode tip (Figure 4b). Circuitry incorporated in the generator allowed continuous monitoring of the impedance of the active part of the electrode. Constant temperature monitoring was ensured by the thermocouple located three centimeters from the needle insertion (Figure 4c and 4d).

Description of the procedure. A total of fifteen tests were performed: six tests were performed on swine mammary and six on human breast tissue, three of each with the Miras PTV electrode and three with the Miras LN electrode, and three tests were performed on liver tissue with the Miras LN electrode. Tissue samples were positioned on the ground pad in a container and partially surrounded by saline. The electrodes were inserted in the middle of the tissue sample and power was applied. The end-point of each ablation procedure was the increase of tissue impedance values (>200 Ω) due to tissue charring. Time, power, impedance and temperature were monitored throughout the entire procedure. Temperature values, as sensed by the thermistor located 3 cm from the tip of the electrodes, were used as indicators of the effectiveness of the procedure.

Histopathological analysis. To assess whether or not the cool-tip RF breast ablation was able to induce a successful coagulation necrosis, freshly excised tissue samples of thermoablated swine mammary tissue were formalin-fixed and prepared for histology. Four μm-thick serial paraffin sections were stained with hematoxylin-eosin and histological analysis performed to identify coagulation necrosis, since previous studies have documented the close correlation between histopathological findings and RF-induced coagulation

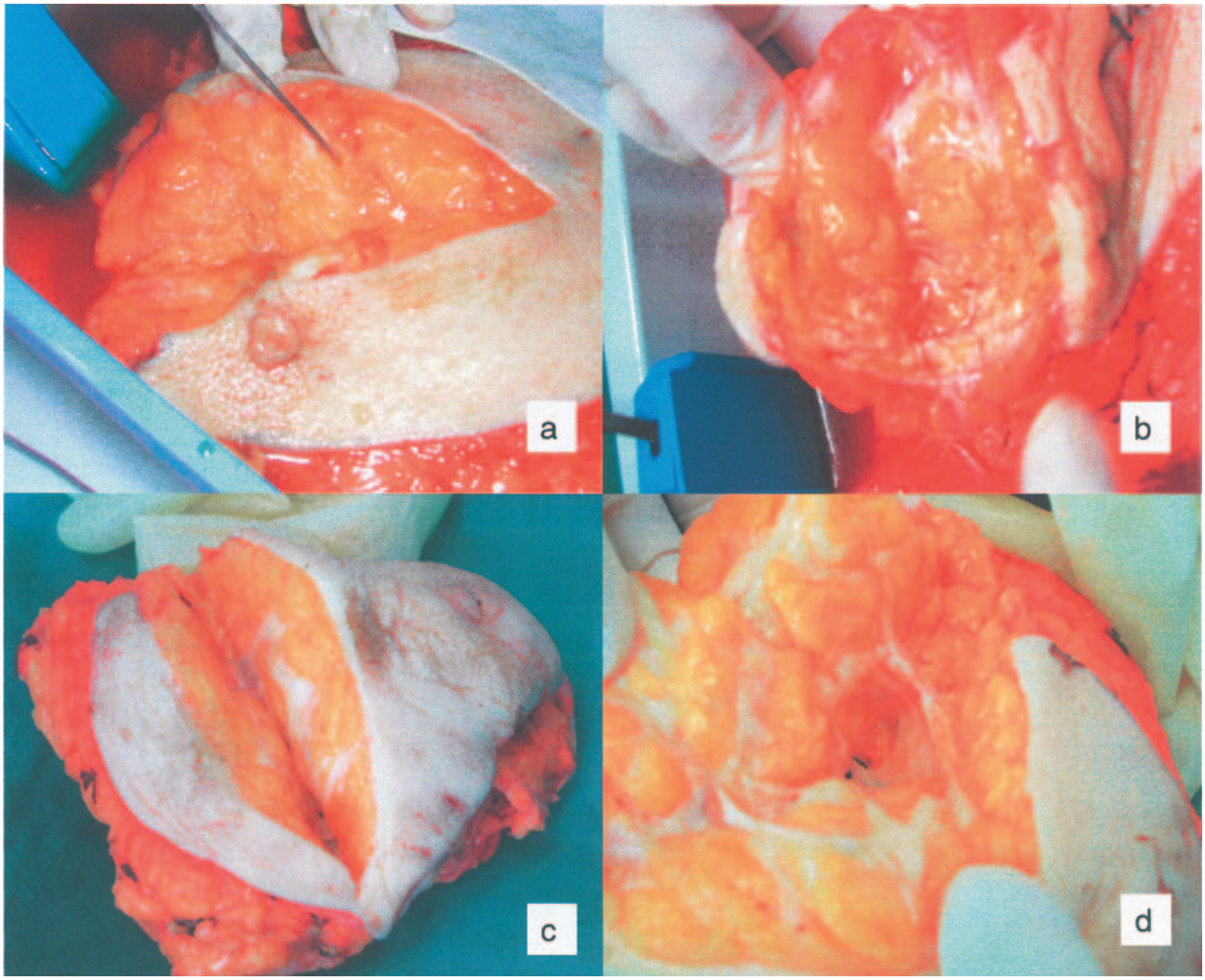

Figure 3. *a) Human breast sample during Miras PTV cool-tip RFA, b) macroscopic appearance of an excised human breast specimen after cool-tip RFA showing the ablated area as a firm whitish tissue with a central needle track surrounded by an area of yellowish coagulated adipose tissue, c) longitudinal cut and d) axial cut of the specimen.*

necrosis (23). Typical signs of the induction of coagulation necrosis, such as the finding of stromal hyalinization with the disappearance of the collagenous fibrillar network, the presence of chromatin migration along the nuclear envelope, nuclear pyknosis and increased cytoplasmic eosinophilia, were recorded (Figure 5).

Results and Discussion

Model 1 versus model 2. In order to assess the efficiency of the multiprobe electrode RF ablation, FEM models of multiprobe RF liver tissue ablation were developed and compared to FEM models of multiprobe RF breast ablation.

Model 1 and model 2 simulate a multiprobe RF breast ablation and a multiprobe RF liver ablation respectively, both with power-controlled mode.

In Model 1, a temperature value of 100˚C was reached in the tissue directly surrounding the hook tips, while temperature values recorded in the tissue located close to the concave areas of the hooks were around 60˚C. Temperature distribution values are shown in Figure 6a (Model 1) and 6b (Model 2).

The *ex vivo* experiments confirmed data from the FEM models (Table II). The differences in ablation time and maximum temperature between mammary and liver tissue recorded with the Miras LN (multiprobe) electrode were substantial (Figures 7 and 8).

Our data demonstrated that, due to the low thermal conductivity of mammary tissue, multiprobe RF breast ablation rapidly induces the charring threshold in the near

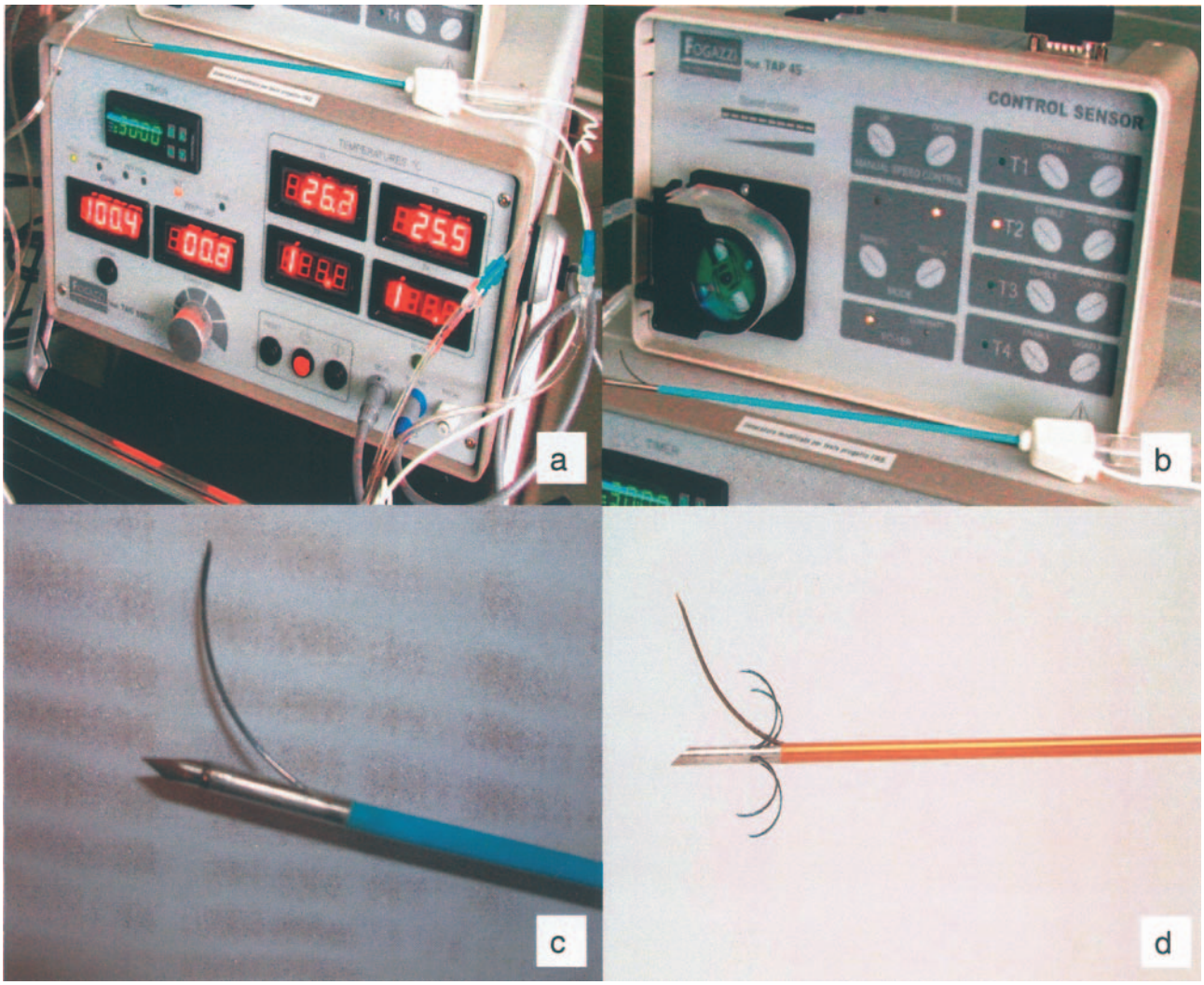

Figure 4. *INVATEC Radiofrequency system: a) TAG100 RF generator, b) cooling Pump, c) Miras PTV cool-tip electrode and d) Miras LN multiprobe electrode.*

proximity of the electrode tip and hooks, thus forcing the procedure to be stopped prematurely before obtaining an adequate ablation volume. On the contrary, multiprobe RF liver ablation, induces heat distribution over larger tissue volumes, probably due to the high liver heat conductivity that favors a more efficient distribution of the temperature within the tissue.

Model 1 versus model 3. Here, model 1 (Figure 6a) is compared to model 3 (Figure 9), which simulates the cool-tip needle RF breast ablation with power-controlled mode. Our data showed that the presence of the cooling moves the maximum temperature values far away from the electrode tip (Figure 9). The temperature distribution was correlated to the tip radius, the power applied and the cooling temperature. In the absence of cooling, the maximum temperature value was located at the tissue-electrode interface, where the resistive heating was usually at its maximum value (Figure 6a).

The model prediction was confirmed by the *ex vivo* procedures performed under the same experimental conditions. The time period necessary to induce the thermal lesion was substantially different between the two electrodes (Table II).

To assess whether or not the cool-tip RF breast ablation was able to induce a successful coagulation necrosis, histo-pathological analysis of a thermoablated swine mammary specimen was performed. Typical signs of the induction of coagulation necrosis were observed with the Miras PTV cool-tip RF as shown in Figure 5.

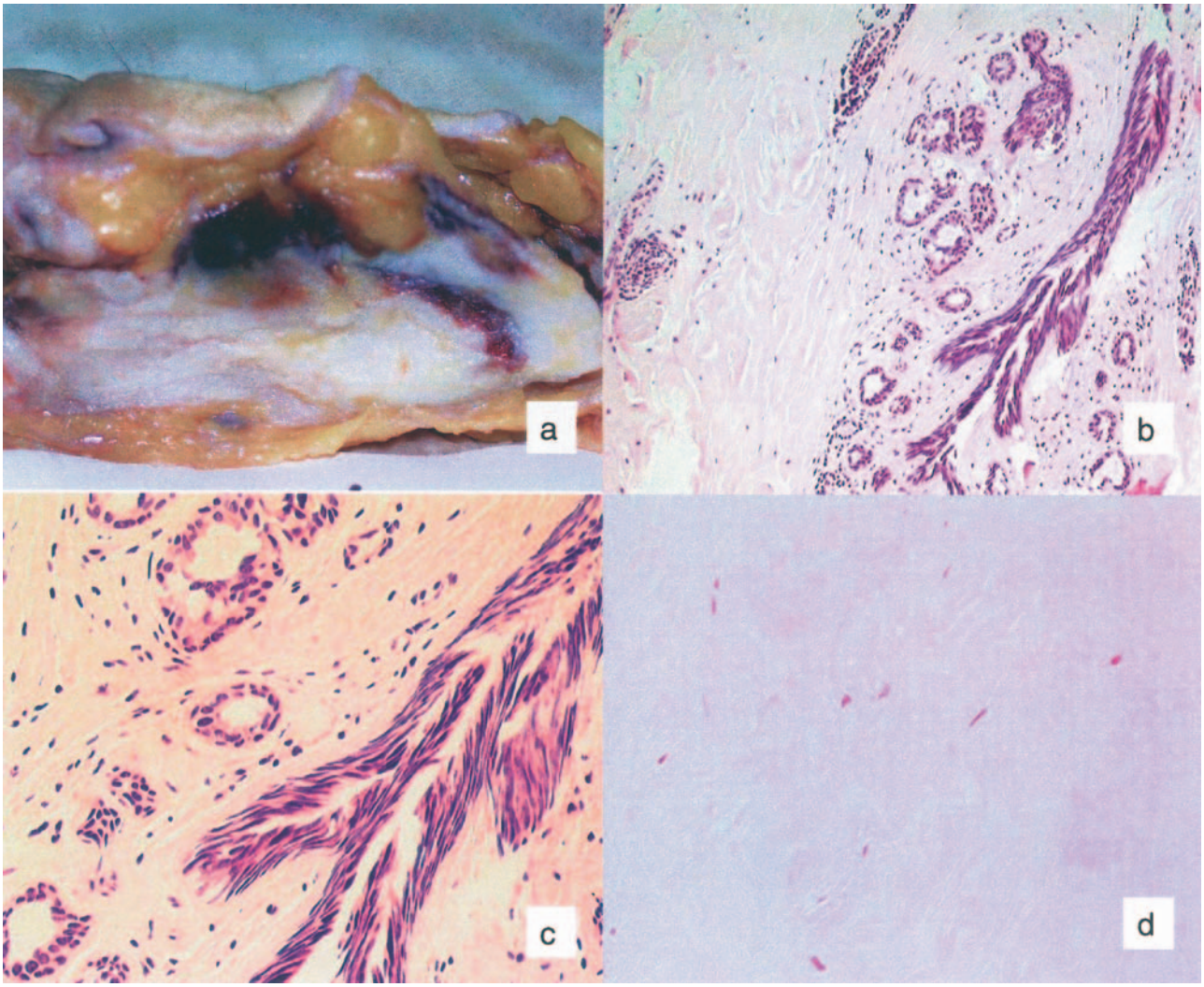

Figure 5. *a) Macroscopic appearance of an excised swine mammary specimen after Miras PTV cool-tip RFA, b) histopathological analysis of a thermoablated swine breast specimen that shows c) chromatin migration along the nuclear envelope, nuclear pyknosis and increased cytoplasmic eosinophilia and d) stromal hyalinization with the disappearance of the collagenous fibrillar network.*

Our data are in agreement with previous reports (13), which have shown that the employment of internally cooled electrodes causes a "heat sink" effect that removes heat closest to the electrode. The removal of heat closest to the electrode allows for greater current deposition without tissue charring or impedance rise, with the consequent distribution of heat over a larger volume of tissue.

Model 4 versus model 5. To confirm the superior performance of cool-tip needle over multiprobe needle RF breast ablation, breast FEM models were also developed with a temperature-controlled mode.

Model 4 simulating multiprobe RF breast ablation (Figure 10a) and model 5 simulating cool-tip RF breast ablation (Figure 10b) correspond to model 1 and 3, respectively, except for the fact that the temperature-controlled mode was used instead of the power-controlled mode. The remaining parameters were left unchanged. In model 4, a power output of 40 W was applied and adjusted to reach (200 sec) and maintain a temperature value of 90˚C. The time ablation period was 480 sec. The last power value applied was maintained until 100˚C was reached within the tissue (charring point). The overall procedure lasted twelve minutes. The tissue located under the hooks reached a temperature below 70˚C at the end of the ablation procedure. Tissue located at the external side of the hooks reached a temperature between 80-90˚C (red-yellow) that extended for a radius of 1.5 cm from the hooks.

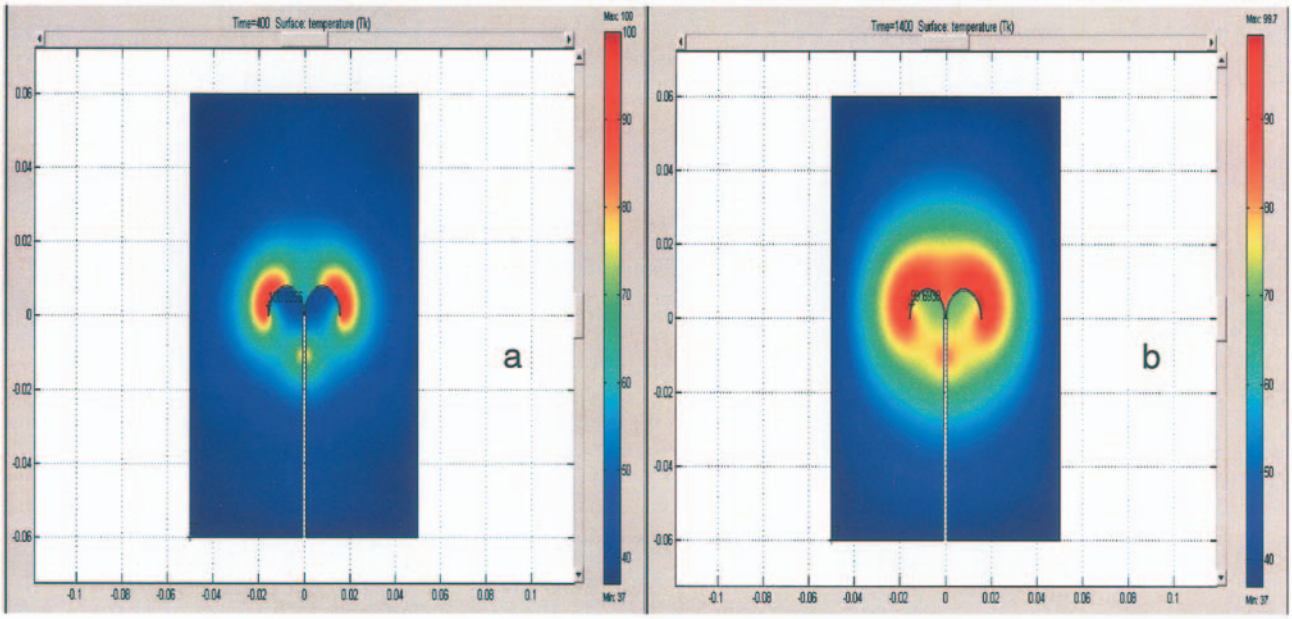

Figure 6. *a) Temperature distribution recorded during power-controlled Miras LN multiprobe RF breast ablation. Power = 30 W; Voltage = 80 V; Time = 400 sec. b) Temperature distribution recorded during power-controlled Miras LN multiprobe RF liver ablation. Power = 30 W; Voltage = 33 V; Time = 1400 sec.*

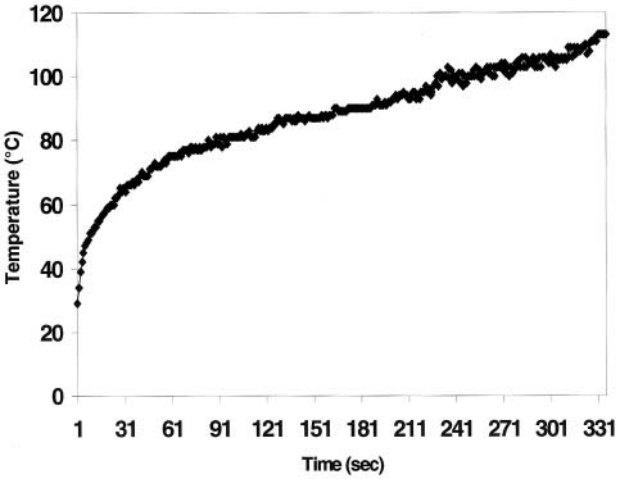

Figure 7. *Experimental ex vivo study: Miras LN multiprobe electrode, swine mammary tissue temperature at 3 cm from the electrode insertion point.*

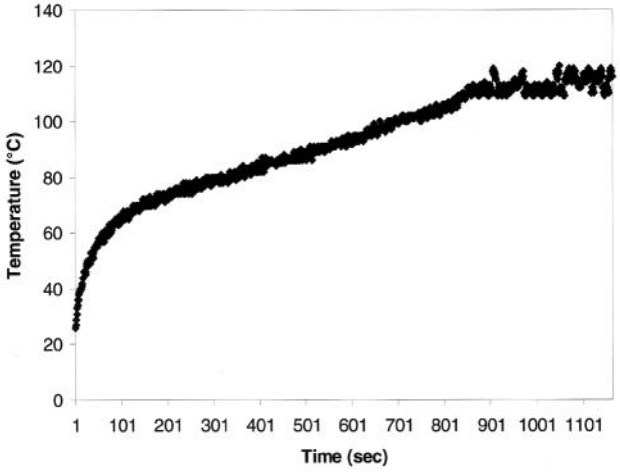

Figure 8. *Experimental ex vivo study: Miras LN multiprobe electrode, liver tissue temperature at 3 cm from the electrode insertion point.*

In model 5, a power output of 30 W was applied and adjusted to maintain a temperature value of 90˚C. The time ablation period was 480 sec. The last power value applied was maintained until 100˚C was reached in the tissue (charring point).

Our data showed that with the temperature-controlled mode cool-tip RF breast ablation created a larger temperature distribution than the multibrobe RF breast ablation (Figure 10a and 10b).

The FEM models developed in this study have demonstrated that cool-tip RF breast ablation assured a higher performance than multiprobe RF breast ablation, both with the power-controlled and the temperature-controlled modes (Figure 9 and Figure 10b).

The potential effects of blood perfusion and temperature dependence of thermal conductivity were not incorporated into our models since it was assumed that they would provide only little additional information. In our study, the FEM breast tissue models were developed with fat only. Our approach was justified due to the fact that fat tissue has a lower conductivity than fibrous or glandular tissue.

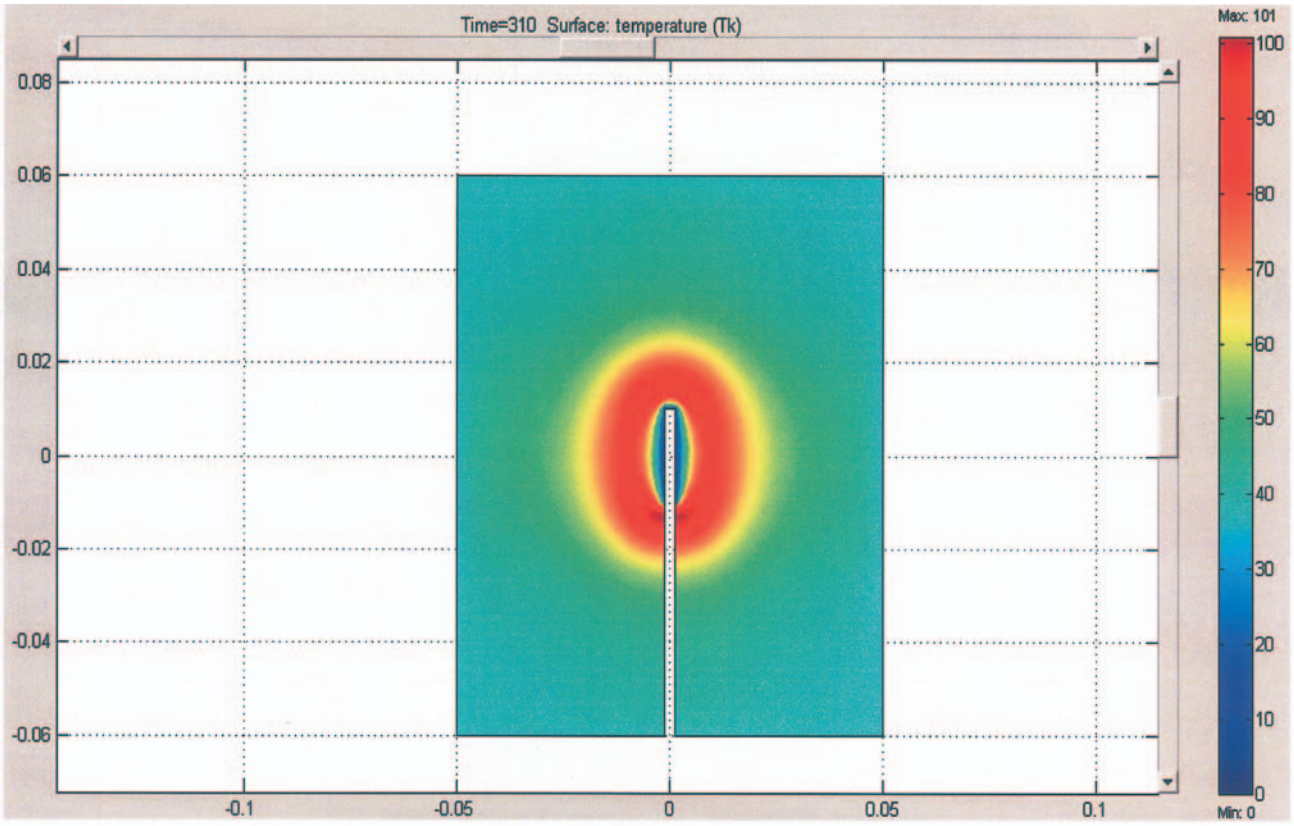

Figure 9. *Temperature distribution recorded during power-controlled Miras PTV cool-tip RF breast ablation. Power = 30 W; Voltage = 140 V; Time = 310 sec.*

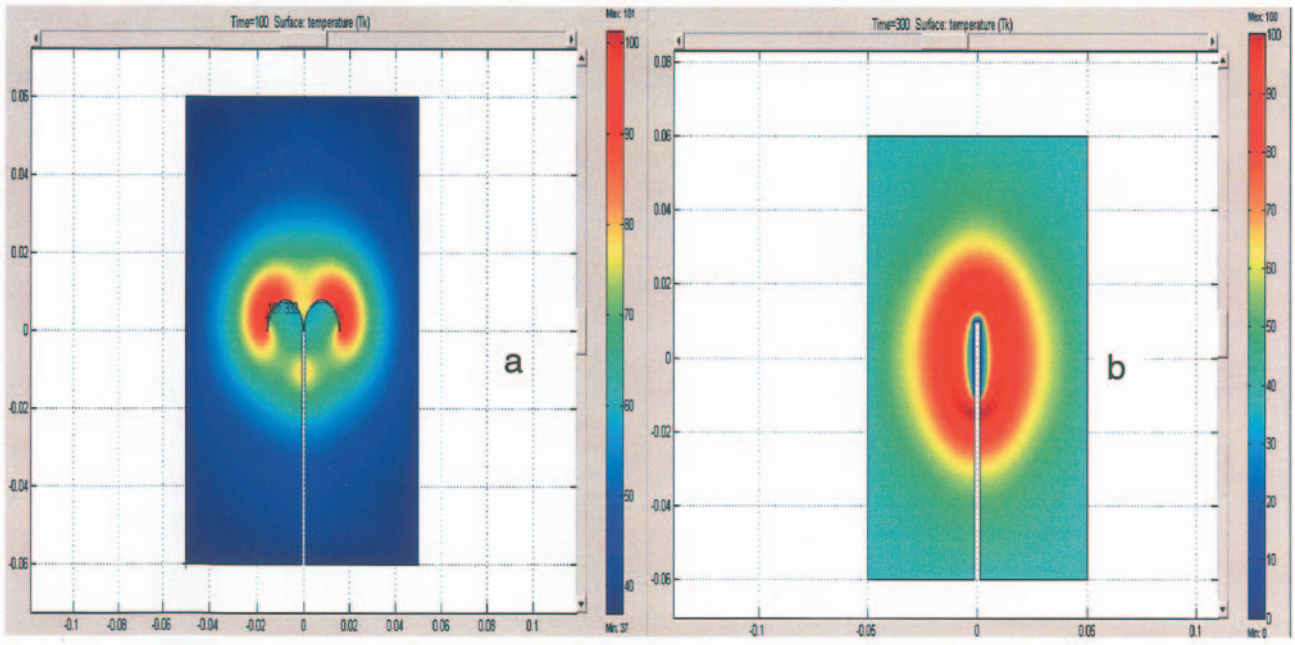

Figure 10. *Temperature distribution recorded a) during temperature controlled Miras LN multiprobe RF breast ablation and b) during temperature-controlled Miras PTV cool-tip RF breast ablation.*

Conclusion

Data from the FEM models developed in this study and from *ex vivo* procedures have shown that cool-tip RF breast ablation assured better performance than multiprobe RF breast ablation in terms of temperature distribution and duration of the procedure.

These differences can probably be attributed to the cooling effect that moves the maximum temperature isotherm far away from electrode tip, inducing heat spread over a larger tissue volume.

Based on our results, it is postulated that in selected cases, treated by experienced personnel, cool-tip RF breast ablation would show optimal oncological results. However, further study of this technique *in vivo* is warranted to determine if it is feasible, safe and capable of producing a sufficient volume of necrosis to be valuable in the treatment of breast malignancies.

References

1 Mizra A, Fornage B, Sneige N, Kuerer H, Newman L, Ames F and Singletary S: Radiofrequency ablation of solid tumors. Cancer J *7(2)*: 95-102, 2001.

2 Martin AP, Goldstein RM, Dempster J *et al*: Radiofrequency thermal ablation of hepatocellular carcinoma before liver transplantation – a clinical and histological examination. Clin Transplant *20(6)*: 695-705, 2006.

3 Goldberg S: Radiofrequency tumor ablation: principles and techniques. Eur J Ultrasound *13(2)*: 129-147, 2001

4 Miller MW and Ziskin MC: Biological consequences of hyperthermia. Ultrasound Med Biol *15*: 707-722, 1989.

5 Lounsberry W, Goldschmidt V and Linke C: The early histological changes following electrocoagulation. Gastrointest Endosc *41*: 68-70, 1995.

6 Geyik S, Akhan O, Abbasoglu O *et al*: Radiofrequency ablation of unresectable hepatic tumors. Diagn Interv Radiol *12(4)*: 195-200, 2006.

7 Izzo F, Thomas R, Delrio P, Rinaldo M, Vallone P, DeChiara A, Botti G, D'Aiuto G, Cortino P and Curley SA: Radiofrequency ablation in patients with primary breast carcinoma. Cancer *92*: 2036-2044, 2001.

8 Burak WE Jr, Agnese DM, Povoski SP, Yanssens TL, Bloom KJ, Wakely PE and Spigos DG: Radiofrequency ablation of invasive breast carcinoma followed by delayed surgical excision. Cancer *98*: 1369-1376, 2003.

9 Hayashi AH, Silver SF, van der Westhuizen NG, Donald JC, Parker C, Fraser S, Ross AC and Olivotto IA: Treatment of invasive breast carcinoma with ultrasound guided radiofrequency ablation. Am J Surg *185*: 429-435, 2003.

10 Fornage BD, Sneige N, Ross MI, Mirza AN, Kuerer HM, Edeiken BS, Ames FC, Newman LA, Babiera GV and Singletary SE: Small (< or = 2- cm) breast cancer treated with US-guided radiofrequency ablation: feasibility study. Radiology *231*: 215-224, 2004.

11 McGahan JP, Gu W-Z, Brock JM, Tesluk H and Jones CD: Hepatic ablation using bipolar radiofrequency electrocautery. Acad Radiol *3*: 418-422, 1996.

12 Goldberg SN, Gazelle GS, Solbiati L, Rittman WJ and Mueller PR: Radio-frequency tissue ablation: increased lesion diameter with a perfusion electrode. Acad Radiol *3*: 636-644, 1996.

13 Lorentzen TA: A cooled needle electrode for radio-frequency tissue ablation: Thermodynamic aspects of improved performance compared with conventional needle design. Acad Radiol *3*: 556-563, 1996.

14 Gabriel C and Gabriel S: Compilation of the dielectric properties of body tissue at RF and Microwave frequencies (www.brooks.af.mil/AFRL/HED/hedr/reports/dielectric/home.html), 2002.

15 Gabriel S, Lau RW and Gabriel C: The dielectric properties of biological tissues: II. Measurements in the frequency range 10 Hz to 20 GHz. Phys Med Biol *41*: 2251-2269, 1996.

16 Chang I: Finite element analysis of hepatic radiofrequency ablation probes using temperature-dependent electrical conductivity. Biomed Eng Online *2*: 12-30, 2003

17 Ekstrand V, Viksell H, Shultz I, Sandstedt B, Rotstein S and Eriksson A: Influence of electrical and thermal properties on RF ablation of breast cancer: is the tumour preferentially heated? Biomed Eng Online *4*: 41-57, 2005.

18 Haemmerich D, Tungjitkusolmun S, Staelin ST, Lee FT Jr, Mahvi DM and Webster JG: Finite-element analysis of hepatic multiple probe radio-frequency ablation. IEEE Trans Biomed Eng *49*: 836-842, 2002.

19 Hammerich D and Webster JG: Automatic control of finite element models for temperature controlled radiofrequency ablation. Biomedical Engineering OnLine *4*: 42-47, 2005.

20 Duck F: Physical properties of tissue – a comprehensive reference book. Academic Press, New York, pp. 167-223, 1990.

21 Valvano JW *et al*: The simultaneous measurement of thermal conductivity, thermal diffusivity and perfusion in small volume of tissue. J Biomech Eng *106*: 192-197, 1984.

22 Valvano JW, Cochran JR and Diller KR: Thermal conductivity and diffusivity of biomaterials measured with self-heating thermistors. Int J Themophys *6*: 301-311, 1985.

23 Bohem T *et al*: Radio-frequency tumor ablation: internally cooled electrode *versus* saline-enhanced technique in an aggressive rabbit tumor model. Radiology *222(3)*: 805-813, 2002.

Received September 29, 2006
Revised December 22, 2006
Accepted January 3, 2007